Resonant Raman Scattering from Amplitude Modes in *trans*-$(CH)_x$ and -$(CD)_x$

Z. Vardeny, E. Ehrenfreund, and O. Brafman
Physics Department and Solid State Institute, Technion, Haifa 32000, Israel

and

B. Horovitz
Department of Nuclear Physics, The Weizmann Institute of Science, Rehovot, Israel

(Received 15 July 1983)

The three resonantly enhanced Raman vibrations in *trans*-$(CH)_x$ and -$(CD)_x$ are described in terms of amplitude modes associated with the Peierls gap. The dispersion in the Raman-line profiles is explained by inhomogeneity. A narrow distribution of the effective electron-phonon coupling constant is required to account for the observed spectra in detail. The resonant Raman vibrations and the ir-active modes induced by doping or photogeneration are all described by the same form of dressed phonon propagator.

PACS numbers: 78.30.Jw, 71.38.+i, 72.80.Le

The resonant Raman scattering (RRS) of both isotopes of polyacetylene reported by several groups[1-5] display characteristic resonance features. As the excitation energy ($\hbar\omega_L$) is changed from red to uv the Raman bands broaden and show a shoulder which shifts to higher frequencies and develops into a prominent satellite peak. In previous studies this "dispersion" was attributed to resonance enhancement due to a distribution of chains with short conjugation lengths.[1-3] Alternatively, Mele proposed[6] that the dispersion is due to hot luminescence in long polyene chains and then the satellite peaks in the RRS spectra are incoherent. Infrared-active vibrations (IRAV) with large oscillator strengths and frequencies different from those measured by RRS were induced in $(CH)_x$ and $(CD)_x$ by doping[1,7] and by photogeneration.[8,9] The two methods yielded different IRAV frequencies.

In this paper we show that all the details of RRS at different $\hbar\omega_L$, as well as doping and photogenerated IRAV for both isotopes, fit into a *single* basic theory. For the first time we provide evidence for identifying the three Raman intrachain vibrations in both $(CH)_x$ and $(CD)_x$ as amplitude modes associated with the Peierls gap. The dispersion in the Raman profile is explained by a narrow distribution in the effective electron-phonon (e-ph) coupling constant.

RRS on free-standing films of *trans* configuration at 300 K, excited with $\hbar\omega_L = 2$ and 2.6 eV, are shown in Fig. 1 for $(CH)_x$ and Fig. 2 for $(CD)_x$. Several features are similar in both compounds. In each of them three resonantly enhanced phonon lines are observed. *The primary* $(CH)_x$ peak frequencies are $\bar{\omega}_1^{H} = 1065$, $\bar{\omega}_2^{H} = 1291$, and $\bar{\omega}_3^{H} = 1460$ cm^{-1}, and correspondingly those of $(CD)_x$ are $\bar{\omega}_1^{D} = 855$, $\bar{\omega}_2^{D} = 1197$, and $\bar{\omega}_3^{D} = 1355$ cm^{-1}. In both compounds the integrated intensity I_2 is smaller than I_1 and I_3. As $\hbar\omega_L$ increases from 2 eV to the uv there emerge shoulders at higher frequencies than the main lines, which gradually develop into prominent satellite peaks.

For each ω_L we deconvolute each Raman line into a symmetric line peaked at the primary frequency and a satellite line. The straight vertical lines in Figs. 1 and 2 point to the satellite frequencies for the respective ω_L. In Fig. 3 we plot

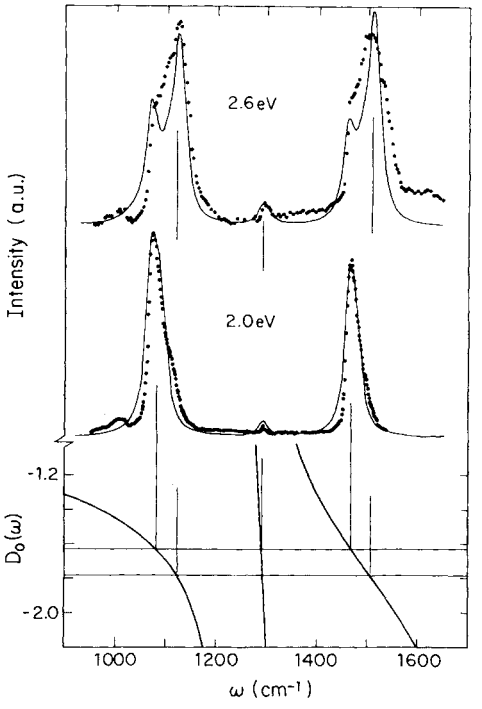

FIG. 1. RRS spectrum of $(CH)_x$ at 300 K. The dots are experimental, full lines are theoretical fit. $D_0(\omega)$ is displayed and the horizontal lines correspond to the two resonance conditions.

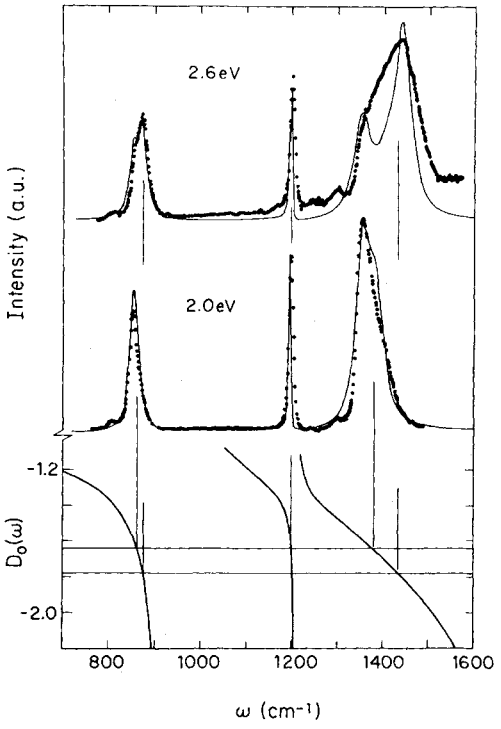

FIG. 2. As in Fig. 1, but for $(CD)_x$.

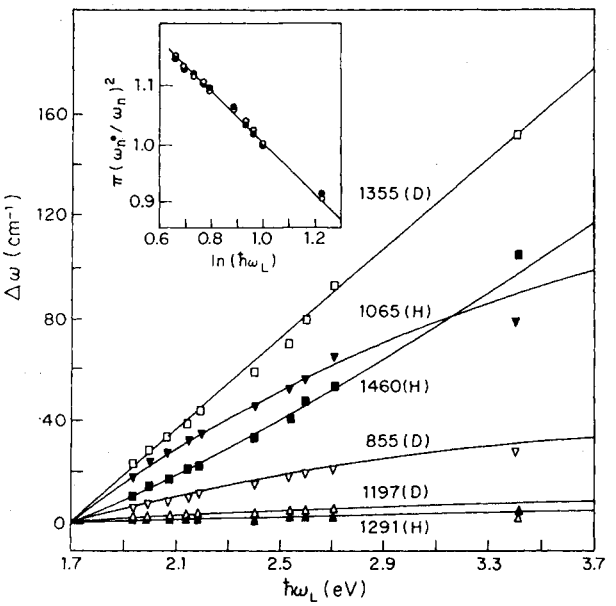

FIG. 3. $\Delta\omega_n$ vs $\hbar\omega_L$ for the six phonons observed by RRS in $(CH)_x$ and $(CD)_x$. Full lines are theoretical; full and empty symbols are experimental for $(CH)_x$ and $(CD)_x$, respectively. Inset: The product $\Pi_{n=1}^{3}(\omega_n^*/\omega_n)^2$ vs $\hbar\omega_L$. (ω_n^* are the satellite frequencies at $\hbar\omega_L = 2.7$ eV.)

the shifts $\Delta\omega_n = \omega_n - \bar{\omega}_n$ of the six satellite frequencies in both $(CH)_x$ and $(CD)_x$ as a function of ω_L. It is seen that $\Delta\omega_n$ and therefore ω_n increase with ω_L; the primary frequency does not change.

The Raman line profiles shown in Figs. 1 and 2 are not unique; the satellite-line relative intensity depends on sample quality.[4,10] This is strong evidence for the presence of inhomogeneity in polyacetylene films and its influence on RRS. Assuming a distribution in the e-ph coupling (caused by the inhomogeneity) we show in the following that the phonon dispersion can be accounted for in a consistent way.

In a one-dimensional (1D) Peierls semiconductor such as polyacetylene,[11] the intrachain vibrations with the highest e-ph coupling can be described in terms of amplitude modes.[12] These are the Raman-active dynamic oscillations around the static configuration of the lattice.[13,14] The cross section $d^2\sigma/d\Omega\, d\omega$ for amplitude-mode RRS is proportional to the dressed phonon propagator,[14,15]

$$\frac{d^2\sigma}{d\Omega\, d\omega} \sim |f(\hbar\omega_L/2\Delta)|^2 \,\mathrm{Im}\,\frac{D_0(\omega)}{1+(1-2\tilde{\lambda})D_0(\omega)}, \quad (1)$$

$$D_0(\omega) = \sum_{n=1}^{N} \frac{\lambda_n}{\lambda}\,\frac{\omega_n^{0\,2}}{\omega^2 - \omega_n^{0\,2} - i\delta_n\omega}. \quad (2)$$

In Eqs. (1) and (2) λ is the dimensionless e-ph interaction coefficient[12] ($\lambda = \sum\lambda_n$), N is the number of coupled phonons (here $N=3$), and ω_n^0 and δ_n are the bare phonon frequencies and their natural linewidth. $\tilde{\lambda}$ is a coefficient which contains e-ph interaction and e-e interaction: $1-2\tilde{\lambda} = 2\lambda E_i''(\Delta_0)$ where E_i'' is the second derivative of the interaction energy. In the Peierls model $\lambda = \tilde{\lambda}$ and the gap is given by[12]

$$2\Delta = 4E_c\exp(-1/2\tilde{\lambda}), \quad (3)$$

where E_c is the electron cutoff energy. The function f^2 in Eq. (1) gives the intensity of the RRS lines as a function of $\hbar\omega_L/2\Delta$. In a purely 1D system and for zero Raman frequency f^2 diverges[15] at $\hbar\omega_L/2\Delta \simeq 1$ as $(\hbar\omega_L/2\Delta - 1)^{-3}$. This strong divergence is suppressed for finite interchain interaction and finite Raman frequencies.[16] The eigenfrequencies of the system are the poles of Eq. (1) and satisfy the equation $D_0(\omega) = -1/(1-2\tilde{\lambda})$.[12]

Using the product rule for amplitude mode vibrations[12] $\Pi_n(\omega_n/\omega_n^0)^2 = 2\tilde{\lambda}$ we conclude from Fig. 3 that $2\tilde{\lambda}$ increases with ω_L. The resonance condition $\hbar\omega_L = 2\Delta$ implies therefore that different $\hbar\omega_L$ are sensitive to regions with different Δ, and Δ increases with $\tilde{\lambda}$ [as, e.g., in Eq. (3)]. To

check the consistency of the Peierls gap equation [Eq. (3)] we plotted in the inset in Fig. 3 the product $\prod_{n=1}^{3}(\omega_n^*/\omega_n)^2$ vs $\ln(\hbar\omega_L)$ for both isotopes, ω_n^* being the satellite frequencies at $\hbar\omega_L = 2.7$ eV. It is clearly seen that this product is isotope independent and indeed linear with $\ln(\hbar\omega_L)$. Using Eq. (3) we obtain $E_c = 6.3$ eV. The good agreement with the Peierls gap equation and the isotope-independent data strongly suggest that the RRS vibrations in polyacetylene are amplitude modes of the Peierls gap.[14,15]

The bare frequencies ω_n^0 and normalized e-ph constants λ_n required to compute $D_0(\omega)$ were obtained by a least-squares fitting procedure to ω_n when excited in the visible range, using $2\tilde{\lambda}$ at resonance from Eq. (3) with $E_c = 6.3$ eV. We found $\omega_1^0 = 1234$, $\lambda_1 = 0.07$, $\omega_2^0 = 1309$, $\lambda_2 = 0.02$, $\omega_3^0 = 2040$ cm^{-1}, and $\lambda_3 = 0.91$ for $(CH)_x$, while $\omega_1^0 = 921$, $\lambda_1 = 0.06$, $\omega_2^0 = 1207$, $\lambda_2 = 0.005$, $\omega_3^0 = 2040$ cm^{-1}, and $\lambda_3 = 0.93$ for $(CD)_x$. The calculated $D_0(\omega)$ for each isotope is plotted in Figs. 1 and 2 showing the way in which the satellite frequencies ω_n increase with $\hbar\omega_L$. At higher $\hbar\omega_L$ resonance conditions are matched by larger 2Δ (and $2\tilde{\lambda}$) so that the horizontal lines drawn at $-1/(1-2\tilde{\lambda})$ intersect $D_0(\omega)$ at higher frequencies. In this way we obtained the $\Delta\omega_n(\omega_L)$ curves for the six phonons of $(CH)_x$ and $(CD)_x$ shown in Fig. 3. The agreement with the experimental $\Delta\omega_n$ values is remarkably good. It is instructive to note that the phonon relative intensities I_n, the linewidths $\delta\omega_n$, and the shifts $\Delta\omega_n$ of the RRS spectrum can all be directly deduced from $D_0(\omega)$. All of them are inversely proportional to the derivative $D' = \partial D_0/\partial\omega$ at $\omega = \omega_n$. For example, in $(CD)_x$, $D'(\omega_2)$ is the highest (Fig. 2) whereas $\Delta\omega_2$, I_2, and $\delta\omega_2$ are the smallest. In $(CH)_x$, $I_1 > I_3 > I_2$ (Fig. 1) while the order is reversed in D'.

The good fit obtained in Fig. 3 shows that we can find a $D_0(\omega)$ such that the satellite frequencies are solutions of $D_0(\omega) = -(1-2\tilde{\lambda})^{-1}$ at different $\tilde{\lambda}$ values. We conclude therefore that the system is inhomogeneous in $\tilde{\lambda}$ with a distribution $P(\tilde{\lambda})$. From nutation NMR experiments[17] there is an indication that a distribution in bond length exists in *trans*-$(CH)_x$ which may be related to variations in chain length. We stress, however, that within our model both the 1D gap (2Δ) and the RRS frequencies are determined uniquely by the Peierls gap equation [Eq. (3)] and amplitude-mode RRS strength [Eq. (1)]. This differs significantly from the previous "conjugation length" model[1-4] in which the gap and the RRS frequencies have been assumed to vary inversely with the chain length.

To obtain the Raman profile at each $\hbar\omega_L$, we integrate the Raman cross section [Eq. (1)] over $P(\tilde{\lambda})$. Because of the sharpness and strength of the RRS cross section for amplitude modes f^2, a single-peak distribution $P(\tilde{\lambda})$ is sufficient to account for the double-peak structure observed in the RRS lines. The primary peak for each phonon line is caused by the peak in $P(\tilde{\lambda})$ while its satellite peak is due to the resonant enhancement f^2 which probes the tail of $P(\tilde{\lambda})$. Therefore the primary frequencies determine the peak of $P(\tilde{\lambda})$ to be at $2\tilde{\lambda} = 0.37$. With use of Eq. (3) this gives a mean 1D gap at $2\Delta = 1.7$ eV in excellent agreement with experiment.[11] To estimate the width of $P(\tilde{\lambda})$ we have chosen for simplicity a Lorentzian function. The theoretical fits shown in Figs. 1 and 2 were obtained with a width of 0.015 for $P(\tilde{\lambda})$, which is surprisingly narrow. These curves were obtained with use of $\delta_1 \simeq \delta_3 \simeq 20$–$30$ cm^{-1}, $\delta_2^{H} \simeq 15$ cm^{-1}, and $\delta_2^{D} \simeq 2$ cm^{-1}, and they give quite satisfactorily all the characteristic dispersion properties: primary and satellite frequencies, relative intensities, and linewidth. We stress here that this yields correctly the peak and the width of $P(\tilde{\lambda})$; its exact shape is still to be determined.

The same $D_0(\omega)$ which describes the RRS results determines also the IRAV frequencies and line shapes when charges are added to the chains,[12] either by doping[1,7] or by photogeneration.[8,9] As previously shown[12] the absorption constant in the phonon frequency range (except for the function f) takes a form similar to Eq. (1), but the eigenfrequencies satisfy $D_0(\omega) = -1/(1-\alpha_p)$, where α_p is a pinning parameter. For polyacetylene $\alpha_p < 2\tilde{\lambda}$,[12] and therefore the IRAV frequencies are lower than those obtained in RRS. In the case of photogeneration (PG) the pinning is weaker than that of doping [α_p(PG) < α_p(DOP)]; therefore the IRAV should show up at lower frequencies for PG, as is indeed observed.[8,9] Since the pinning potential is not known, a single IRAV experimental frequency with the same $D_0(\omega)$ used for RRS fixes α_p. Once this is done, all other eigenfrequencies fit excellently the experimental values, as shown in Table I. Note that the missing experimental PG line in the table is predicted to be at 1216 cm^{-1}. However, since $D'(1216)$ is large (Fig. 2) the relative intensity should be small (calculated: $I_2/I_3 \sim 15$).

In conclusion, we have demonstrated that RRS in *trans*-polyacetylene of both isotopes can be described in terms of amplitude modes together with a narrow shaped distribution in the parame-

TABLE I. Induced ir-active phonon frequencies (in inverse centimeters) by doping (DOP) or photogeneration (PG). ω_i^{H}, $(CH)_x$; ω_i^{D}, $(CD)_x$.

Phonon frequency	DOP ($\alpha_p = 0.23$) Theor.	Expt.[1]	PG ($\alpha_p \simeq 0.06$) Theor.	Expt.[8,9]
ω_1^{H}	886	888	488	500
ω_2^{H}	1285	1288	1278	1275
ω_3^{H}	1397	1397	1364	1365
ω_1^{D}	770	790	410	400
ω_2^{D}	1148	1140	1045	1045
ω_3^{D}	1236	1240	1216	•••

ter $\tilde{\lambda}$. The same dressed-phonon propagator describes equally well the ir-active modes induced by doping and by photogeneration. We have therefore linked together these various experiments in the same general theory.

Note added.—The missing PG line in Table I was discovered at 1224 cm^{-1} with the predicted relative intensity.[18]

[1]I. Harada, Y. Furukawa, M. Tasumi, H. Shirakawa, and S. Ikeda, J. Chem. Phys. 73, 4746 (1980).

[2]E. Mulazzi, G. P. Brivio, E. Faulques, and S. Lefrant, Solid State Commun. 46, 851 (1983).

[3]H. Kuzmany, E. A. Imhoff, D. B. Fitchen, and A. Sarhangi, Phys. Rev. B 26, 7109 (1982).

[4]D. B. Fitchen, Mol. Cryst. Liq. Cryst. 83, 1127 (1982).

[5]L. Lauchlan *et al.*, Phys. Rev. B 27, 2307 (1983).

[6]E. J. Mele, Solid State Commun. 44, 827 (1982).

[7]S. Etemad *et al.*, Phys. Rev. B 23, 5137 (1981).

[8]Z. Vardeny, J. Orenstein, and G. L. Baker, Phys. Rev. Lett. 50, 2032 (1983).

[9]G. B. Blanchet, C. R. Fincher, T. C. Chung, and A. J. Heeger, Phys. Rev. Lett. 50, 1938 (1983).

[10]P. Knoll, H. Kuzmany, P. Surjan, and M. Kertesz, to be published.

[11]A. J. Heeger and A. G. MacDiarmid, Mol. Cryst. Liq. Cryst. 77, 1 (1981).

[12]B. Horovitz, Solid State Commun. 41, 729 (1982).

[13]M. J. Rice, Phys. Rev. Lett. 37, 36 (1976).

[14]B. Horovitz, H. Gutfreund, and M. Weger, Phys. Rev. B 17, 2796 (1978).

[15]B. Horovitz, to be published.

[16]To account for the interchain coupling we truncate smoothly the function f^2 at $|\hbar\omega_L - 2\Delta| \cong 0.15$ eV leaving only a finite peak at $\hbar\omega_L = 2\Delta$.

[17]C. S. Yannoni and T. C. Clarke, Phys. Rev. Lett. 51, 1191 (1983).

[18]Z. Vardeny, Phys. Rev. Lett. 51, 1221 (1983).